Schweizerischer Erdbebendienst
Service Sismologique Suisse
Servizio Sismico Svizzero
Servizi da Terratrembels Svizzer

ETH
Eidgenössische Technische Hochschule Zürich
Swiss Federal Institute of Technology Zurich

Sierre - Borzuat (SIEB)

SITE CHARACTERIZATION REPORT

Clotaire MICHEL, Valerio POGGI, Daniel ROTEN,

Jan BURJANEK, Carlo CAUZZI, Donat FÄH

Sonneggstrasse 5 CH-8092 Zürich Switzerland; E-mail: clotaire.michel@sed.ethz.ch

Last modified : October 15, 2013

Abstract

Ambient vibration array measurements were performed to characterize the alluvial fan at site Sierre Borzuat. This area, where the new station SIEB of the Swiss Strong Motion Network was installed, underwent high damages during the 1946 earthquake, the most recent damaging in the Valais region [Fritsche and Fäh, 2009]. In order to characterize the velocity profile under the station, array measurements with an aperture of $200\,\mathrm{m}$ were performed. The measurements were successful and allowed deriving a velocity model for this site. The soil column underlying station SIEB displays a strong gradient in the top $20\,\mathrm{m}$, with shear-velocities increasing from approximately 200 to $1000\,\mathrm{m/s}$. A layer with constant velocity extends down to about $65\,\mathrm{m}$. At this depth, a clear interface is found, with a velocity of the lower layer around $1500-1700\,\mathrm{m/s}$. The velocity increases slightly with depth until a velocity contrast at about $200\,\mathrm{m}$ depth, which is interpreted as the sediment-bedrock interface. $V_{s,30}$ is equal to $730\,\mathrm{m/s}$, corresponding to ground type B for EC8 [CEN, 2004] and SIA261 [SIA, 2003], i.e. much firmer than expected from the official ground type map (class C). The theoretical SH transfer function and impedance contrast of the quarter-wavelength velocity computed from the inverted profiles show large amplification at high frequencies (above $10\,\mathrm{Hz}$), and moderate amplification at the fundamental resonance frequency ($2.4\,\mathrm{Hz}$). Recordings of the new station will allow to validate these 1D models.

Contents

1 Introduction

The station SIEB (Sierre - Borzuat) is part of the Swiss Strong Motion Network (SSMNet) in the Valais. SIEB has been newly installed in the framework of the SSMNet Renewal project in 2012. This project includes also the site characterization. The passive array measurements have been selected as a standard tool to investigate these sites. Such a measurement campaign was carried out on 9th August 2012 around the school Borzuat (Fig. 1), with a centre close to station SIEB, in order to characterize the sediments under this station. The last heavy damaging earthquake (M close to 6) in Switzerland occurred in Sierre in 1946. Damage was particularly noticeable in two districts of the city: Beaulieu (array SIDE) and ND des Marais (this study) [Fritsche and Fäh, 2009]. According to the geological map, this station is located on an alluvial fan on top of the deep Rhone valley. More precisely, the map indicates a Quaternary colluvial deposit there. This layer, extremely loose, explains the name of the church located inside the array "Notre-Dame des Marais" (swamps). This report presents the measurement setup, the results of the H/V analysis and of the array processing of the surface waves (dispersion curves). Then, an inversion of these results into velocity profiles is performed. Standard parameters are derived to evaluate the amplification at this site.

Canton	City	Location	Station code	Site type	Slope
Valais	Sierre	Borzuat	SIEB	Alluvial fan	Slight slope

Table 1: Main characteristics of the study-site.

Figure 1: Picture of the site.

2 Experiment description

2.1 Ambient Vibrations

The ground surface is permanently subjected to ambient vibrations due to:

- natural sources (ocean and large-scale atmospheric phenomena) below $1\,\mathrm{Hz}$,
- local meteorological conditions (wind and rain) at frequencies around $1\,\mathrm{Hz}$,
- human activities (industrial machines, traffic…) at frequencies above $1\,\mathrm{Hz}$ [Bonnefoy-Claudet et al., 2006].

The objective of the measurements is to record these ambient vibrations and to use their propagation properties to infer the underground structure. First, the polarization of the recorded waves (H/V ratio) is used to derive the resonance frequencies of the soil column. Second, the arrival time delays at many different stations are used to derive the velocity of surface waves at different frequencies (dispersion). The information (H/V, dispersion curves) is then used to derive the properties of the soil column using an inversion process.

2.2 Equipment

For these measurements 12 Quanterra Q330 dataloggers named NR01 to NR12 and 14 Lennartz 3C 5 s seismometers were available (see Tab. 2). Each datalogger can record on 2 ports A (channels EH1, EH2, EH3 for Z, N, E directions) and B (channels EH4, EH5, EH6 for Z, N, E directions). Time synchronization was ensured by GPS. The sensors were placed on a metal tripod on firm soil or asphalt, ensuring a good coupling with the ground.

Digitizer	**Model**	**Number**	**Resolution**
	Quanterra Q330	12	$24\,\mathrm{bits}$
Sensor type	**Model**	**Number**	**Cut-off frequency**
Velocimeter	Lennartz 3C	14	$0.2\,\mathrm{Hz}$

Table 2: Equipment used.

2.3 Geometry of the arrays

The array configuration is made of 3 rings of 20, 50 and $100\,\mathrm{m}$ radius around a central station (14 sensors). The minimum inter-station distance and the aperture are therefore 20 and $200\,\mathrm{m}$. The experimental setup is displayed in Fig. 2. The final usable dataset is detailed in section 3.2.

Figure 2: Geometry of the arrays.

2.4 Positioning of the stations

The sensor coordinates were measured using a differential GPS device (Leica Viva GS10), including only a rover station and using the Real Time Kinematic technique provided by Swisstopo. It allowed an absolute positioning with an accuracy better than $5\,\mathrm{cm}$ on the Swissgrid except for points SIE203 and SIE303 with a precision of 20 and $27\,\mathrm{cm}$, respectively. This precision was assumed sufficient for this processing. Moreover, point SIE304 was located by measuring $3\,\mathrm{m}$ East from its actual position using compass and measuring tape, which means that its actual precision is in the order of $10\,\mathrm{cm}$.

3 Data quality

3.1 Usable data

The largest time windows were extracted, for which all the sensors of the array were correctly placed and the GPS synchronization was ensured. The array was limited in size by the main road in the South, where the traffic was not negligible. A light wind was blowing during the measurements. GPS measurements were not performed during the recordings to avoid additional noise. Few cars crossed the array during the recordings.

The north-alignment of the sensors was double-checked by maximizing the correlation with the central station at low frequencies (between 1 and 3 Hz here) [Poggi et al., 2012b]. Deviation of $21\,^\circ$ was found for SIE204 and around $\pm 10\,^\circ$ at points SIE103, SIE202, SIE205, SIE301 and SIE305. Original and rotated datasets are available for the array analysis.

The spectra show that points SIE302 has a particularly high noise level in the Vertical and East directions compared to the other points due to the road in the South. Moreover, horizontal directions of point SIE303 are amplified above 3 Hz with peaks at 3.4, 4.4 and 7.8 Hz due to the fact that the point was located on a retaining wall. This point may be removed from future analysis, even though it was used for the analysis described in this report.

The characteristics of the datasets are detailed in Tab. 3.

3.2 Data processing

The data were first converted to SAC format including header entries for the point coordinates (CH1903 system), the recording component and a name related to the position. The name is made of 3 letters characterizing the location (SIE here), 1 digit for the ring and 2 more digits for the number in the ring. Recordings were not corrected for instrumental response.

Dataset	Starting Date	Time	Length	F_s	Min. inter-distance	Aperture	# of points
1	2012/08/09	12:15	123 min	200 Hz	20 m	200 m	14

Table 3: Usable datasets.

4 H/V processing

4.1 Processing method and parameters

In order to process the H/V spectral ratios, several codes and methods were used. The classical H/V method was applied using the Geopsy `http://www.geopsy.org` software. In this method, the ratio of the smoothed Fourier Transform of selected time windows are averaged. Tukey windows (cosine taper of 5% width) of $50\,\mathrm{s}$ long overlapping by 50% were selected. The Konno and Ohmachi [1998] smoothing procedure was used with a b value of 80. The classical method computed using the method of Fäh et al. [2001] was also performed.

Moreover, the time-frequency analysis method [Fäh et al., 2009] was used to estimate the ellipticity function more accurately using the Matlab code of V. Poggi, available in the software repository of the engineering seismology group of SED. In this method, the time-frequency analysis using the Wavelet transform is computed for each component. For each frequency, the maxima over time (10 per minute with at least $0.1\,\mathrm{s}$ between each) in the TFA are determined. The Horizontal to Vertical ratio of amplitudes for each maximum is then computed and statistical properties for each frequency are derived. A Cosine wavelet with parameter 9 is used. The mean of the distribution for each frequency is stored. For the sake of comparison, the time-frequency analysis of Fäh et al. [2001], based on the spectrogram, was also used, as well as the wavelet-based TFA coded in Geopsy.

The ellipticity extraction using the Capon analysis [Poggi and Fäh, 2010] (see section on array analysis) were also performed.

Method	Freq. band	Win. length	Anti-trig.	Overlap	Smoothing
Standard H/V Geopsy	$0.2 - 20\,\mathrm{Hz}$	$50\,\mathrm{s}$	No	50%	K&O 80
Standard H/V D. Fäh	$0.2 - 20\,\mathrm{Hz}$	$30\,\mathrm{s}$	No	75%	-
H/V TFA Geopsy	$0.2 - 20\,\mathrm{Hz}$	Morlet m=8 fi=1	No	-	-
H/V TFA D. Fäh	$0.2 - 20\,\mathrm{Hz}$	Specgram	No	-	-
H/V TFA V. Poggi	$0.2 - 20\,\mathrm{Hz}$	Cosine wpar=9	No	-	2D MA 10

Table 4: Methods and parameters used for the H/V processing.

4.2 Results

The curves have similar shapes without clear peak (Fig. 4). As explained before, SIE303, located on a retaining wall, provides irrelevant results. All H/V curves show a bump with a peak frequency around $0.6 - 0.7\,\mathrm{Hz}$ that could be related to the wind that was blowing during the measurement or to a deep and weak contrast. Station XSID1, installed during a week in a transformer house close to the centre of the array, shows a tiny peak at $0.7\,\mathrm{Hz}$ and an unclear peak at $2.4\,\mathrm{Hz}$. In the array data, an unclear peak also appears around $2.7\,\mathrm{Hz}$, with little variability that may not be significant. Moreover, Fritsche and Fäh [2009] made an extensive H/V study in Sierre. They generally recognize two peaks in the spectra, one below $1\,\mathrm{Hz}$ and one above. It is doubtful whether the first peak can be recognized in the measurements presented here, since wind may hide the informations at these frequencies. However, the second peak

corresponds to the values found here. Fig. 5 shows all the available H/V data (second peak) available in the zone.

All the methods to compute H/V ratios are compared at the array centre on Fig. 6, in which the classical methods were divided by $\sqrt{2}$ to correct from the Love wave contribution [Fäh et al., 2001]. The small peak is then clearer, with some small differences among the methods. The 3C FK analysis (Capon method) does not have resolution down to the peak, but provides similar results.

The peak at the SIEB station is therefore at $2.4\,\mathrm{Hz}$, with a small peak amplitude (around 2) and another vey small frequency peak at $0.7\,\mathrm{Hz}$. This last peak may be due to the Rhone basin 2D/3D resonance [Fritsche and Fäh, 2009]. However, no particular polarization of the ground motion was observed.

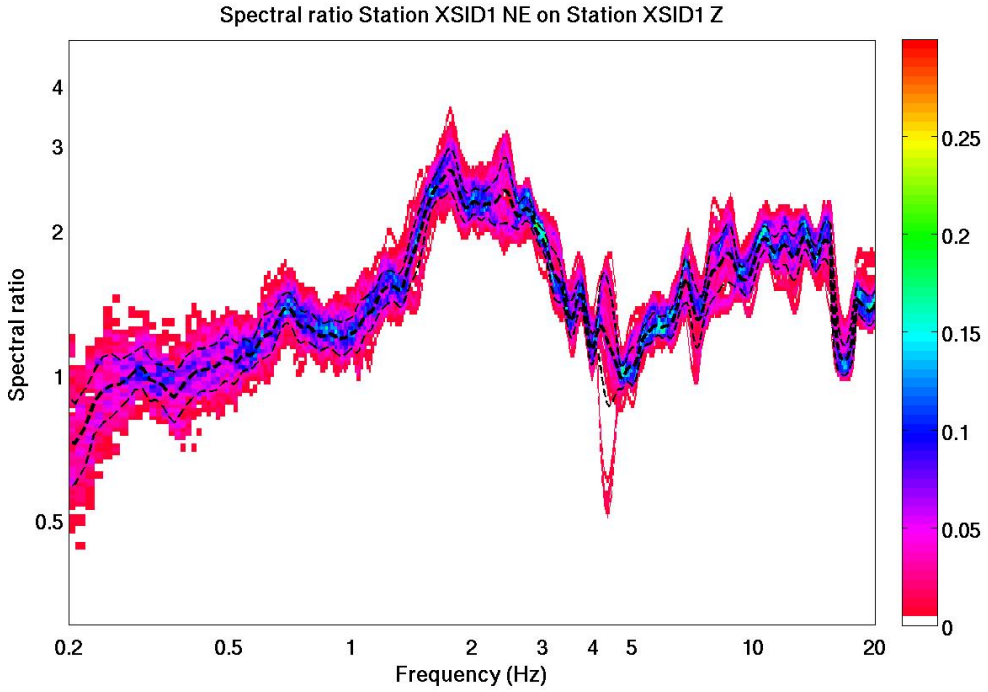

Figure 3: H/V spectral ratios on a long term recording at station XSID1, located close to the array centre

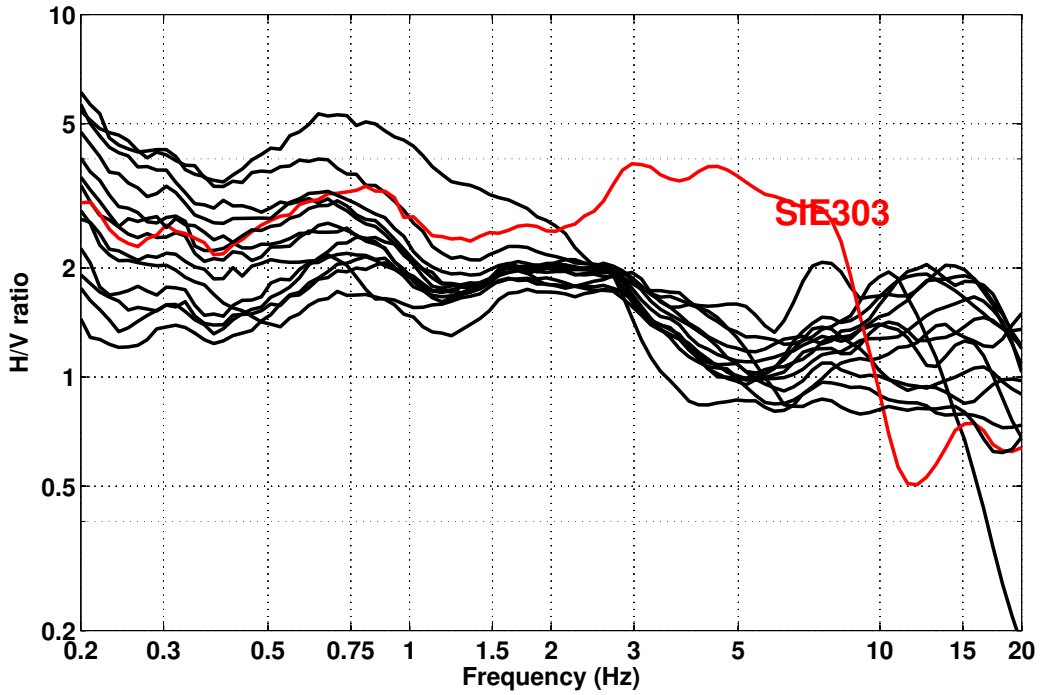

Figure 4: H/V spectral ratios (time-frequency analysis code V. Poggi).

Figure 5: Map of all available H/V frequency peak (second peak) in the area, including points from Fritsche and Fäh [2009].

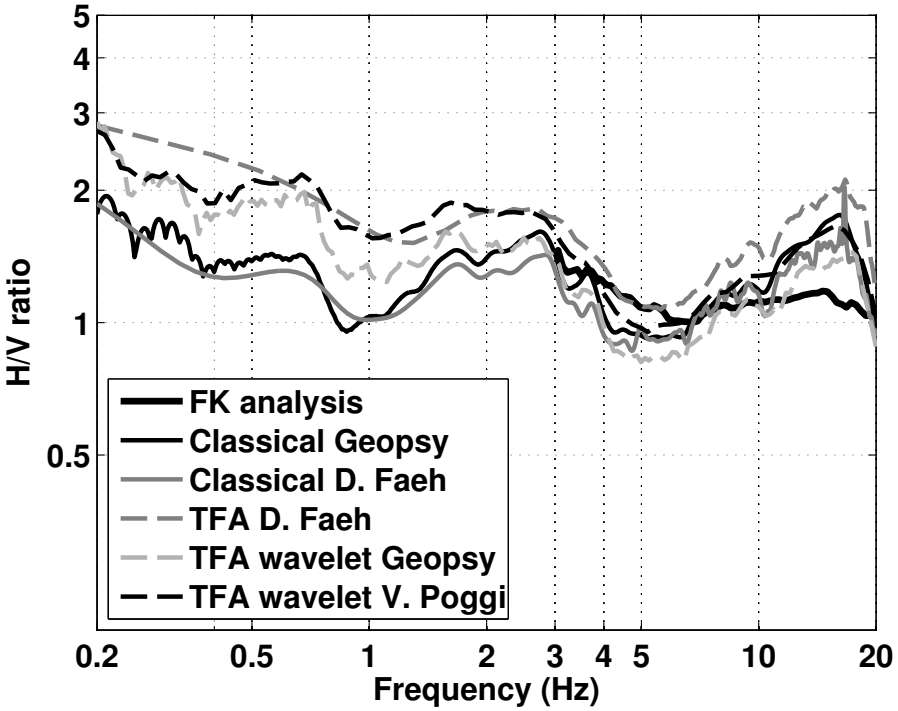

Figure 6: H/V spectral ratios for point SIE000 using the different codes. Classical methods were divided by $\sqrt{2}$.

5 Array processing

5.1 Processing methods and parameters

The vertical components of the arrays were processed using the FK and the High-resolution FK analysis [Capon, 1969] using the Geopsy `http://www.geopsy.org` software. Better results were obtained using large time windows (300T). The results of computations of both datasets were merged to estimate the dispersion curves.

Moreover, a 3C array analysis [Fäh et al., 2008] was also performed using the array_tool_3C software [Poggi and Fäh, 2010]. It allows to derive Rayleigh and Love modes including the Rayleigh ellipticity. The results of computations of both datasets were merged to estimate the dispersion curves.

Method	Set	Freq. band	Win. length	Anti-trig.	Overlap	Grid step	Grid size	# max.
HRFK 1C	1	$1.5 - 30\,\mathrm{Hz}$	$300T$	No	50%	0.001	0.6	5
HRFK 3C	1	$1.5 - 25\,\mathrm{Hz}$	Wav. 10	No	50%	300	3000	5
			Tap. 0.2			m/s	m/s	

Table 5: Methods and parameters used for the array processing.

5.2 Obtained dispersion curves

The first mode (Rayleigh) in the 1C FK analysis could be picked between 3 and $15\,\mathrm{Hz}$ (Fig. 7) including its standard deviation. The dispersion curve can be followed below the lower array limit thanks to the Capon technique. The velocities are ranging from $2000\,\mathrm{m/s}$ at $3\,\mathrm{Hz}$ down to $860\,\mathrm{m/s}$ at $15\,\mathrm{Hz}$. The first upper mode can also be partially picked.

Using the 3C analysis, both fundamental Rayleigh and Love modes can be picked (Fig. 7). Phase velocity of the fundamental mode of Rayleigh wave identified from the 3C analysis shows little difference with respect to the phase velocity picked from 1C analysis (Fig. 8). Rayleigh fundamental mode is picked from 3.4 to $14.6\,\mathrm{Hz}$ and Love from 2.8 to $12.7\,\mathrm{Hz}$ (Fig. 8).

Another array was performed at site SIDE in 2007 [Fritsche and Fäh, 2009], with a centre located $900\,\mathrm{m}$ towards SW (Fig. 9). SIDE and SIEB arrays were performed in the two districts of the city with the most extensive damage in 1946 (Beaulieu and ND des Marais). The fundamental and first higher Rayleigh and Love modes are available, even though Fritsche and Fäh [2009] did not interpret them. The comparison of Rayleigh and Love fundamental dispersion curves with these measurements (Fig. 10) shows a shift in the frequencies and velocities indicating probably a difference in the depth and velocities of the considered interface. Velocities seems lower at SIDE, even though the dispersion curves are available only on a narrow frequency range. Only an inversion of these curves would allow a comparison of these two sites.

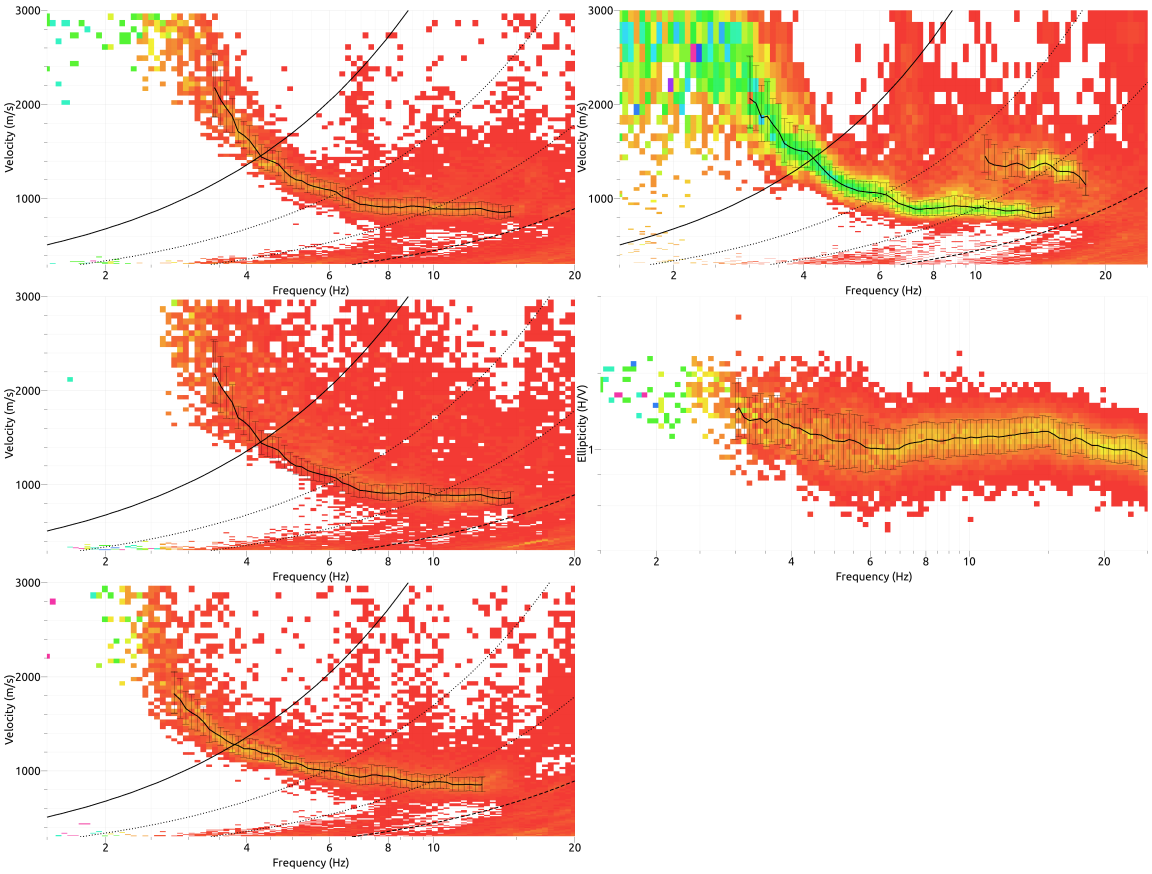

Figure 7: Dispersion curves obtained from the 3C (left) and 1C (right) array analysis (top: vertical, centre: radial, bottom: transverse) and ellipticity from the 3C analysis (centre left).

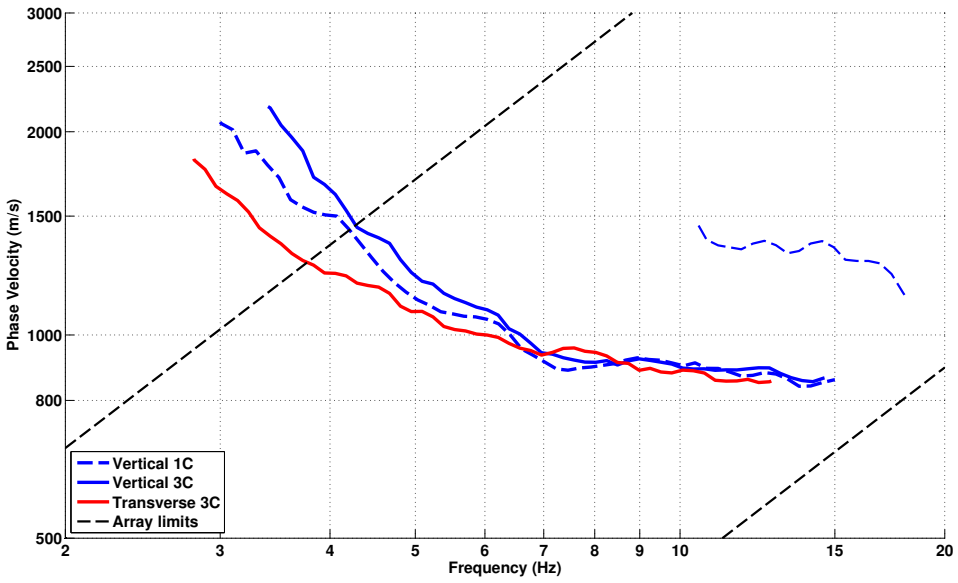

Figure 8: Dispersion curves obtained with the different methods.

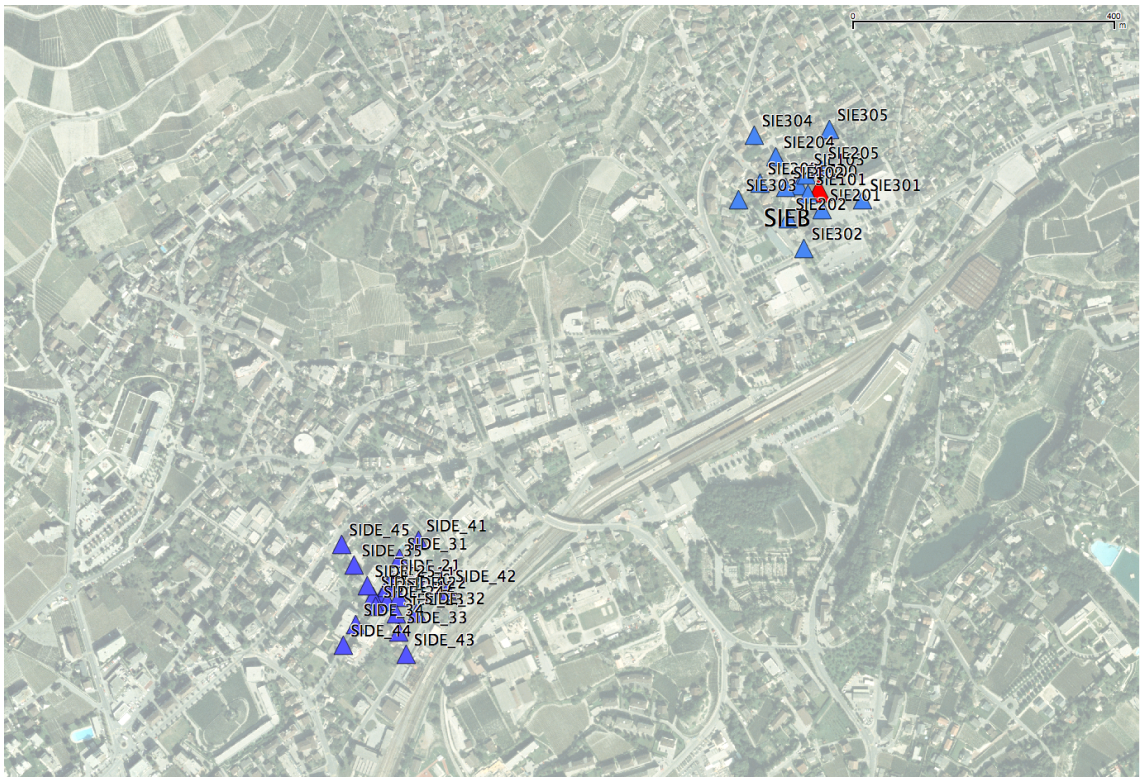

Figure 9: Location of the SIEB and the SIDE arrays in Sierre.

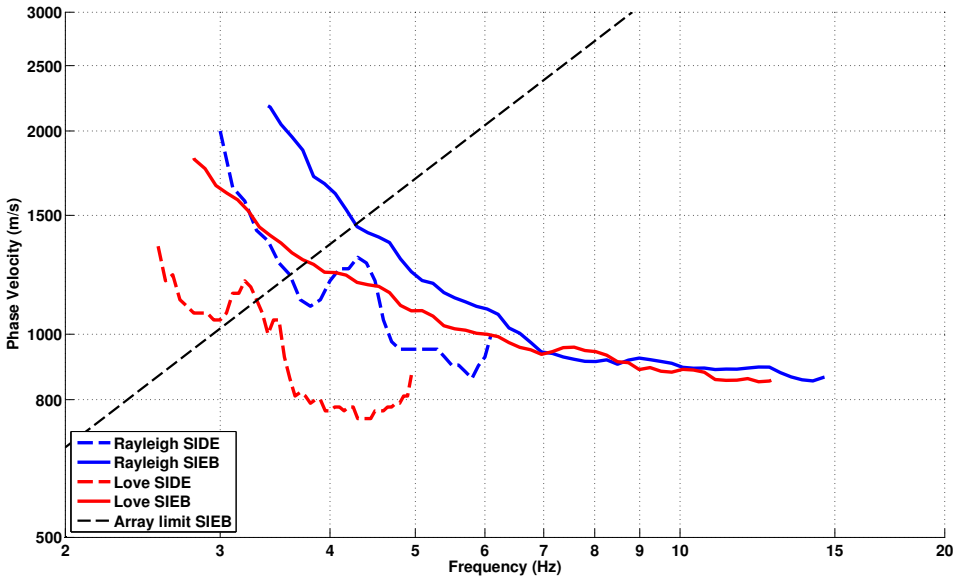

Figure 10: Comparison of the fundamental Rayleigh and Love modes at SIDE array and this study for SIEB station.

6 Inversion and interpretation

6.1 Inversion

For the inversion, dispersion curves of the Rayleigh and Love fundamental and Rayleigh first higher modes, as well as the ellipticity of Rayleigh waves and the ellipticity peak were used as simultaneous targets. No standard deviation was used to avoid different weighting. The results from the 3C FK analysis were used except for the upper Rayleigh mode, where the 1C results were chosen. A weight of 0.05 was assigned to the ellipticity curve and 0.1 to the ellipticity peak at $2.4\,\mathrm{Hz}$. All curves were resampled using 50 points between 1 and $20\,\mathrm{Hz}$ in log scale. The $0.7\,\mathrm{Hz}$ peak may be due to the Rhone basin 2D/3D resonance and was therefore not used [Fritsche and Fäh, 2009].

The inversion was performed using the Improved Neighborhood Algorithm (NA) Wathelet [2008] implemented in the Dinver software. In this algorithm, the tuning parameters are the following: Ns_0 is the number of starting models, randomly distributed in the parameter space, Nr is the the number of best cells considered around these Ns_0 models, Ns is the number of new cells generated in the neighborhood of the Nr cells (Ns/Nr per cell) and It_{max} is the number of iteration of this process. The process ends with $Ns_0 + Nr * \frac{Ns}{Nr} * It_{max}$ models. The used parameters are detailed in Tab. 6.

It_{max}	Ns_0	Ns	Nr
500	10000	100	100

Table 6: Tuning parameters of Neighborhood Algorithm.

During the inversion process, low velocity zones were not allowed. The Poisson ratio was inverted in each layer in the range 0.2-0.4, up to 0.47 below the possible water table. The density was supposed equal to $2000\,\mathrm{kg/m^3}$ except for the layers assumed to be rock ($2500\,\mathrm{kg/m^3}$). Inversions with free layer depths as well as fixed layer depths were performed. 4 layers are enough to explain most of the targets (dispersion and ellipticity), but more layers are used to smooth the obtained results and better explore the parameter space. 5 independent runs of 5 different parametrization schemes (5 and 6 layers over a half space and 11, 13 and 16 layers with fixed depth) were performed. For further elaborations, the best models of these 25 runs were selected (Fig. 14).

On the first $20\,\mathrm{m}$, a gradual increase in the shear-wave velocity is found from low velocities ($200 - 300\,\mathrm{m/s}$, badly constrained) to $1000\,\mathrm{m/s}$ at $20\,\mathrm{m}$ depth. This layer extends down to approximately $65\,\mathrm{m}$ with a constant velocity. At this depth, a clear interface is found, with a velocity of the lower layer around $1500 - 1700\,\mathrm{m/s}$. The velocity increases slightly with depth until what is supposed to be the bedrock. Using the free depth strategy, the bedrock needs to be around $180 - 200\,\mathrm{m}$ depth, whereas the fixed layer depth does not need this interface, but can simply go deeper with the same structure. The bedrock velocity ($3000\,\mathrm{m/s}$) is not trusted. According to Rosselli, the bedrock depth in the region is around $200\,\mathrm{m}$ but the accuracy is poor.

When comparing to the target curves (Fig. 12 and Fig. 13), all curves are well represented. Even though the interface at $65\,\mathrm{m}$ is producing a peak around $2.5\,\mathrm{Hz}$, the layers below are needed to fit the data.

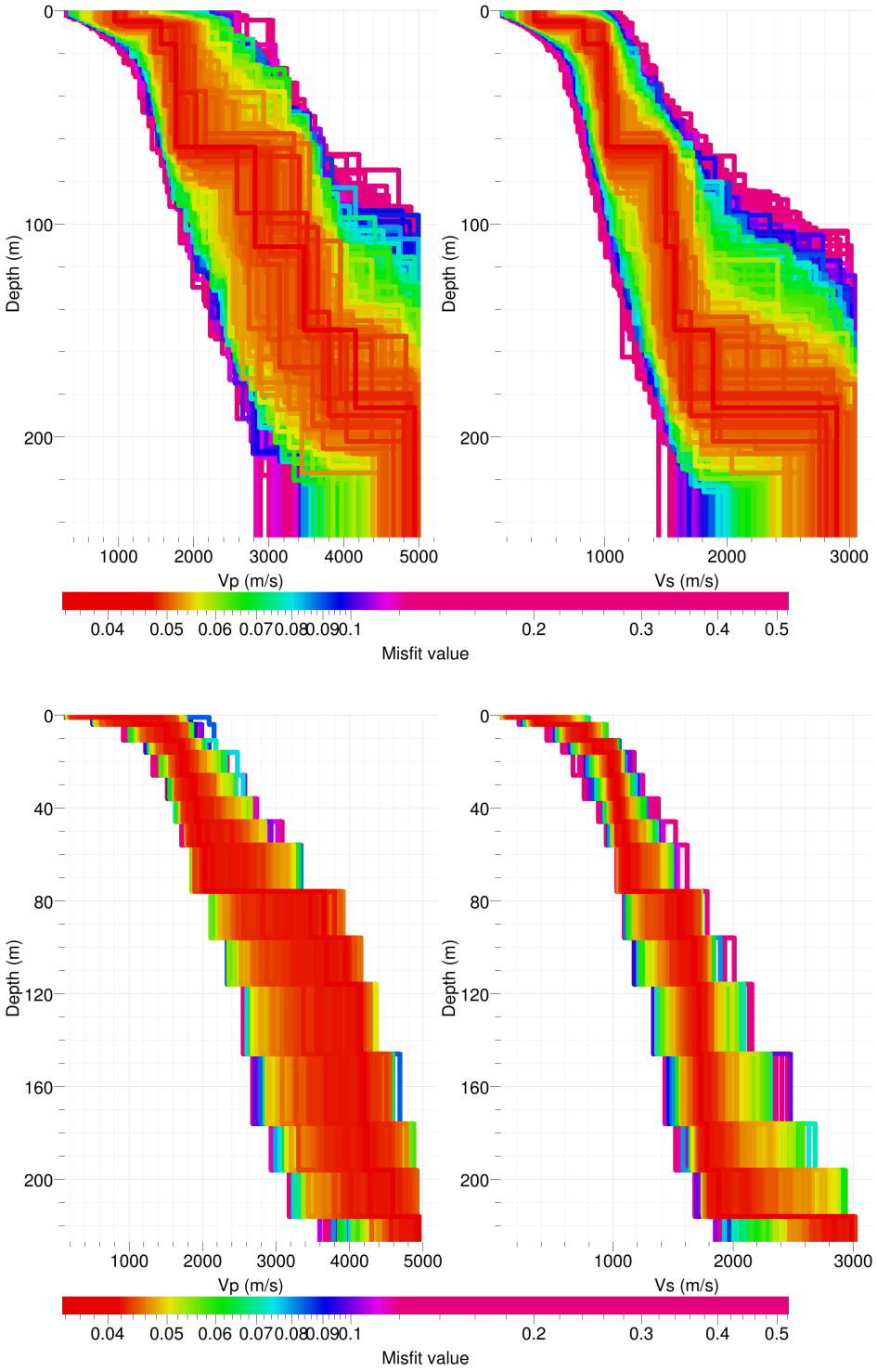

Figure 11: Inverted ground profiles in terms of V_p and V_s; top: free layer depth strategy; bottom: fixed layer depth strategy.

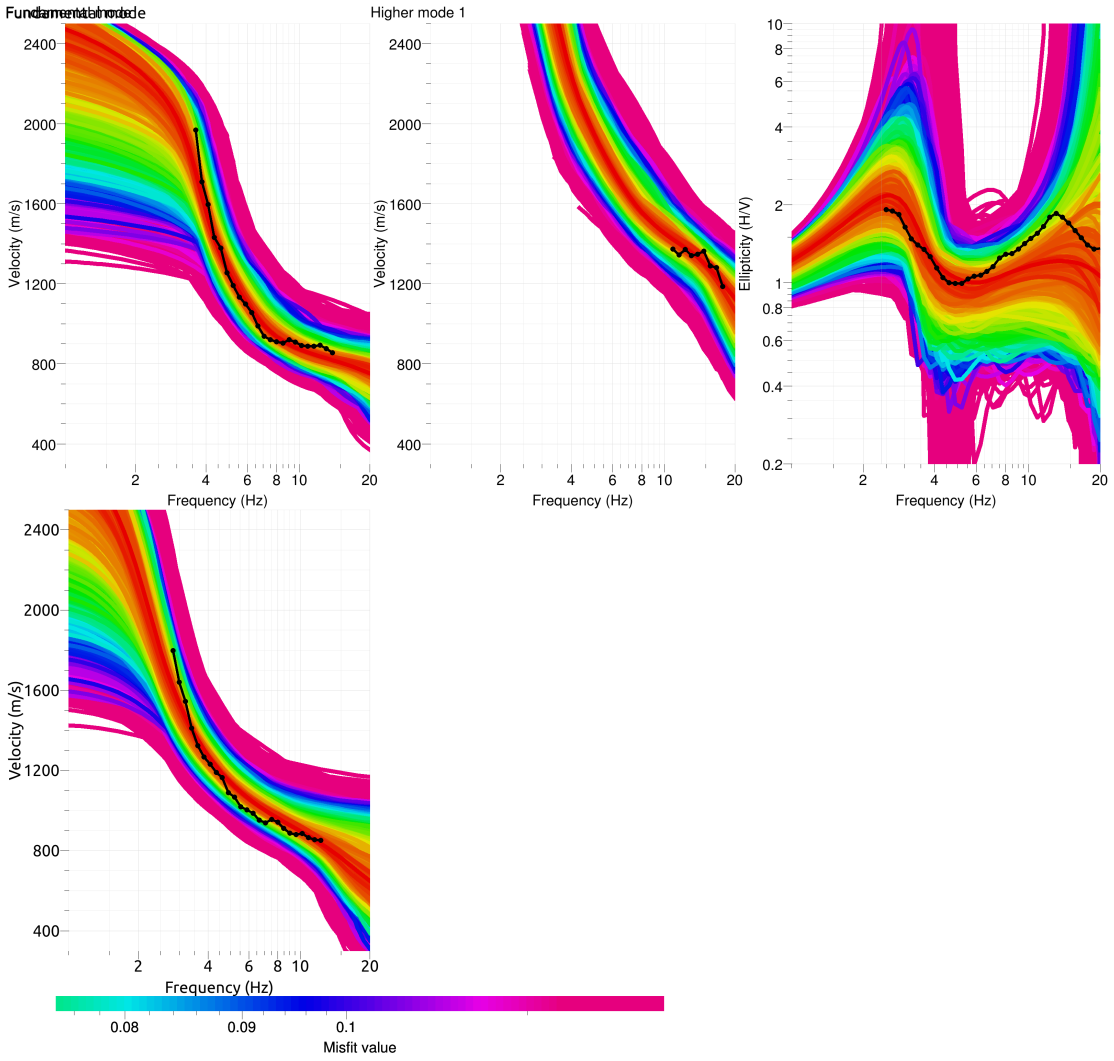

Figure 12: Comparison between inverted models and measured Rayleigh and Love modes and corresponding ellipticity, free layer depth strategy.

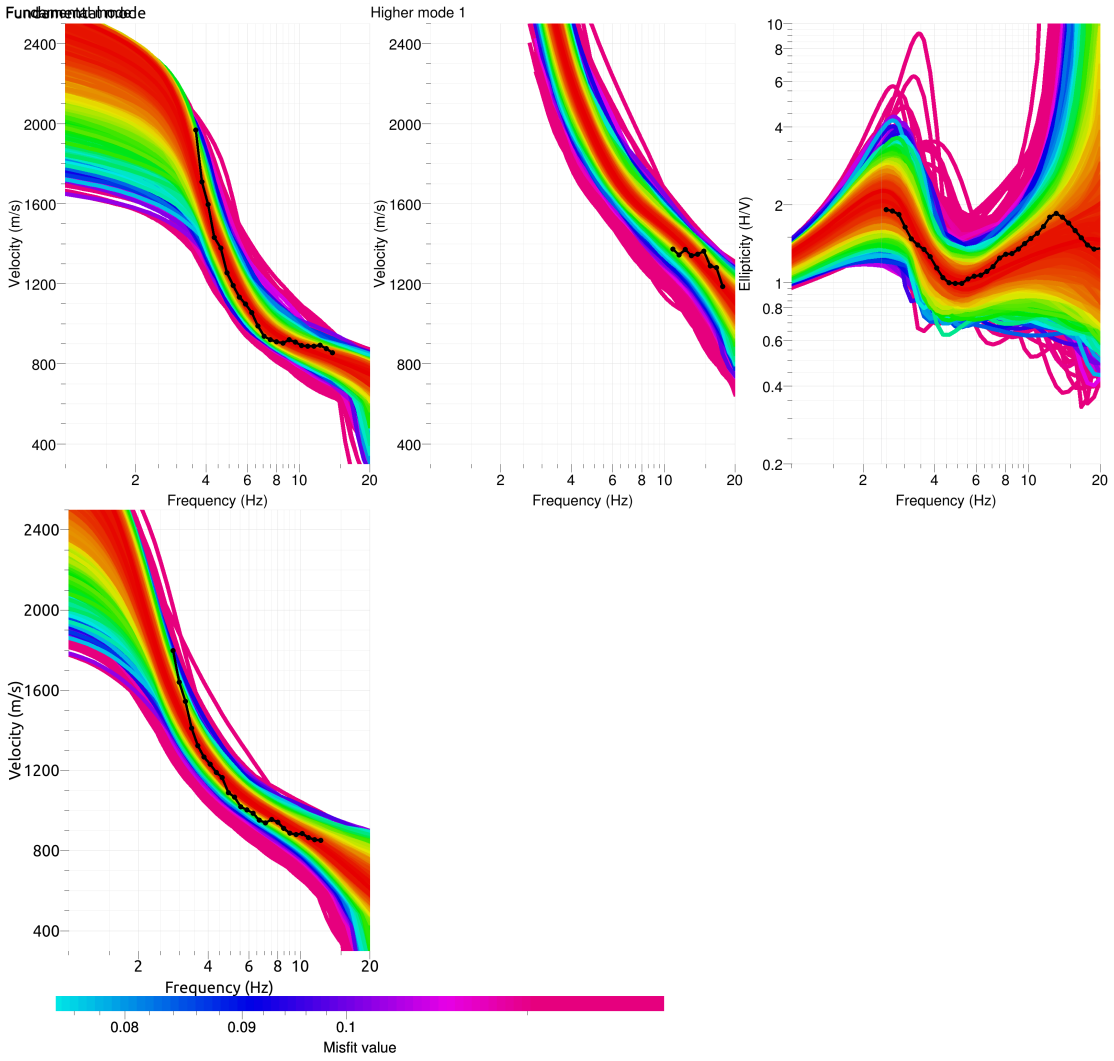

Figure 13: Comparison between inverted models and measured Rayleigh and Love modes and corresponding ellipticity, fixed layer depth strategy.

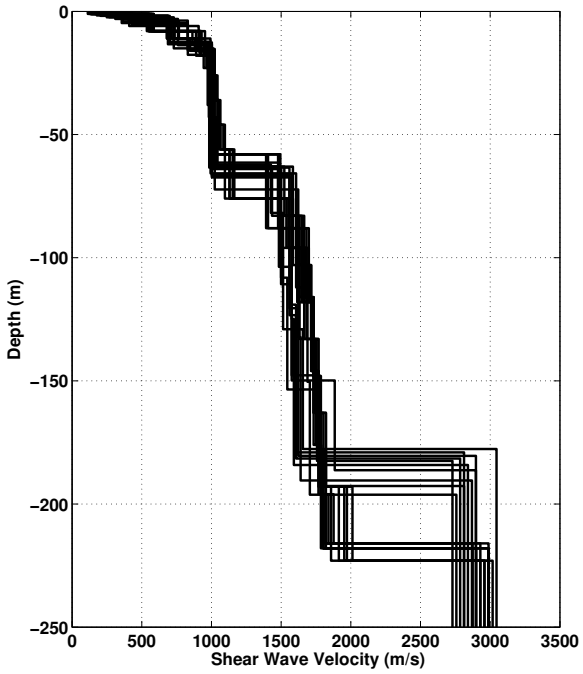

Figure 14: V_s ground profiles for the selected 25 best models.

6.2 Travel time average velocities and ground type

The distribution of the travel time average velocities at different depths was computed from the selected models. The uncertainty, computed as the standard deviation of the distribution of travel time average velocities for the considered models, is also provided, but its meaning is doubtful. $V_{s,30}$ is found to be around $730\,\mathrm{m/s}$, meaning the site can be classified as class B in the Eurocode 8 [CEN, 2004] and SIA261 [SIA, 2003]. For class E, the upper soft layer is not thick enough (less than $5\,\mathrm{m}$). According to the map of ground types from the Federal Office for Environment (`http://map.bafu.admin.ch`), this site is located on site class C (SIA261). It shows once more that the shear wave velocities of alluvial fans are much underestimated.

6.3 SH transfer function and quarter-wavelength velocity

The quarter-wavelength velocity approach [Joyner et al., 1981] provides, for a given frequency, the average velocity at a depth corresponding to 1/4 of the wavelength of interest. It is useful to identify the frequency limits of the experimental data (minimum frequency in ellipticity - $2.5\,\mathrm{Hz}$ - and dispersion curves - $2.8\,\mathrm{Hz}$). The results using this proxy show that no data is controlling the results below $100\,\mathrm{m}$, and the dispersion curves are constraining the results down to $80\,\mathrm{m}$ (Fig. 15). It explains why the velocity is well constrained even below the $65\,\mathrm{m}$ interface. Moreover, the quarter wavelength impedance-contrast introduced by Poggi et al. [2012a] is also displayed in the figure. It corresponds to the ratio between two quarter-wavelength average velocities, respectively from the top and the bottom part of the velocity profile, at a given

	Mean (m/s)	**Uncertainty (m/s)**
$V_{s,5}$	378	42
$V_{s,10}$	492	45
$V_{s,20}$	639	32
$V_{s,30}$	726	29
$V_{s,40}$	780	27
$V_{s,50}$	818	25
$V_{s,100}$	1015	13
$V_{s,150}$	1166	13
$V_{s,200}$	-	-

Table 7: Travel time averages at different depths from the inverted models. Uncertainty is given as one standard deviation from the selected profiles.

frequency [Poggi et al., 2012a]. It shows a trough (inverse shows a peak) at the resonance frequency.

Moreover, the theoretical SH-wave transfer function for vertical propagation [Roesset, 1970] is computed from the inverted profiles. It is compared to the quarter-wavelength amplification [Joyner et al., 1981], that however cannot take resonances into account (Fig. 16). In this case, the models are predicting an amplification up to a factor of 4-5 above $10\,\mathrm{Hz}$, but only 2-3 at the resonance frequencies (2.4 and $4.7\,\mathrm{Hz}$). This will be compared to observations at this station.

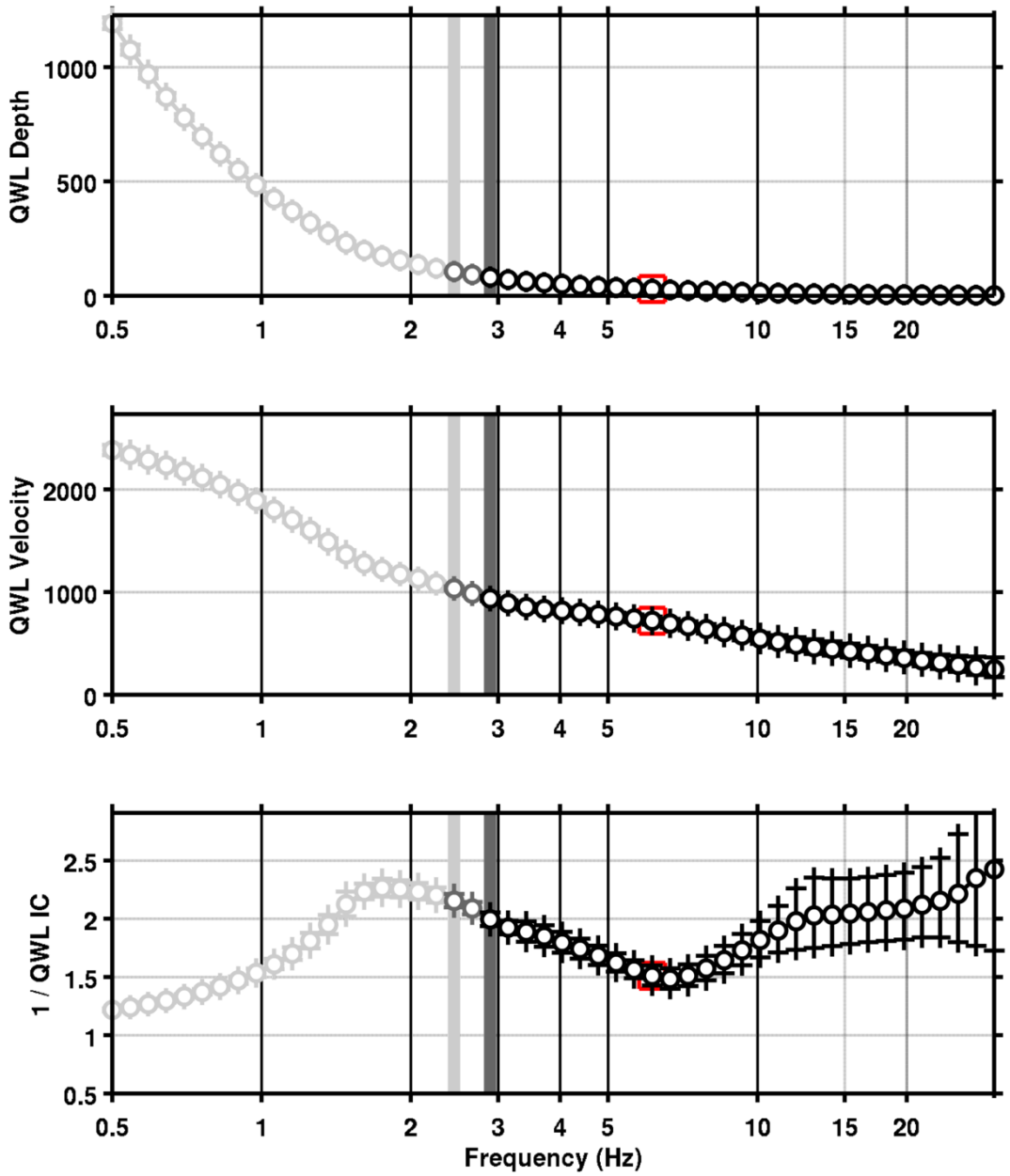

Figure 15: Quarter wavelength velocity representation of the velocity profile (top: depth, centre: velocity, bottom: inverse of the impedance contrast). Black curve is constrained by the dispersion curves, light grey is not constrained by the data. Red square is corresponding to $V_{s,30}$.

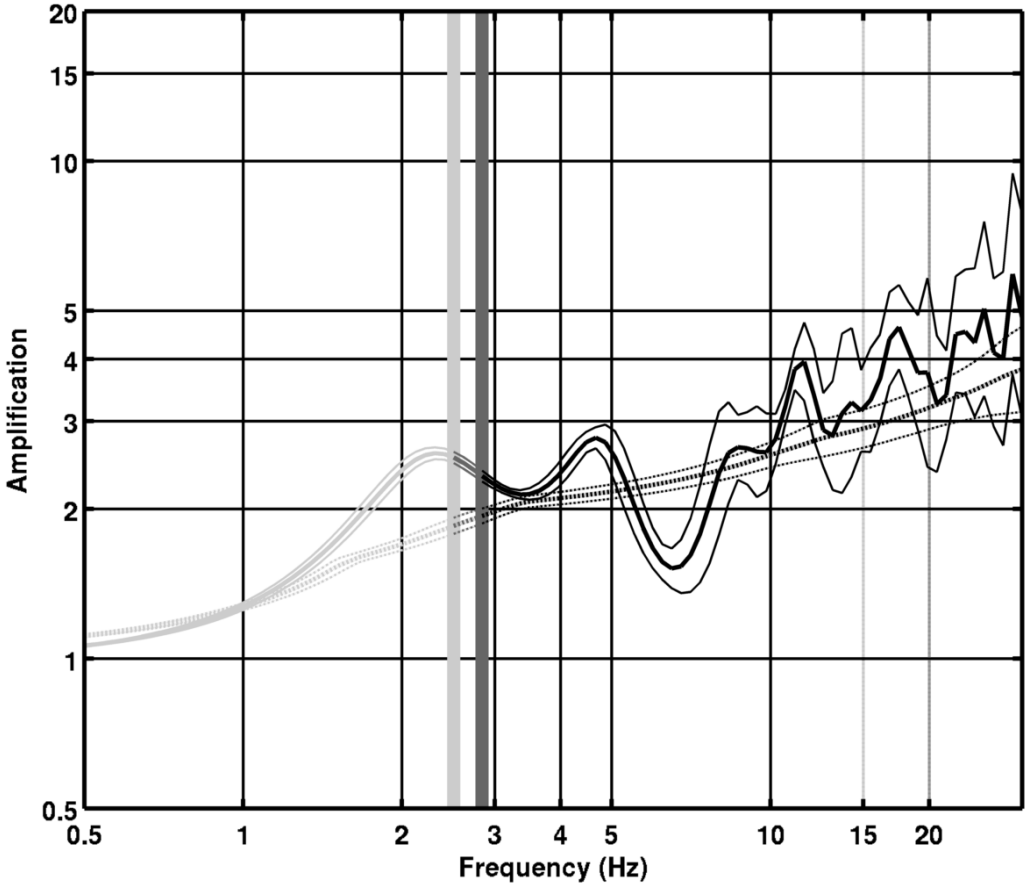

Figure 16: Theoretical SH transfer function (solid line) and quarter wavelength impedance contrast (dashed line) with their standard deviation. Significance of the greyshades is detailed in Fig. 15.

7 Conclusions

The array measurements presented in this study were successful in deriving a velocity model for the Borzuat site in Sierre, below the SIEB station. On the first $20\,\mathrm{m}$, a strong gradient in the velocity is found from $200-300\,\mathrm{m/s}$ to $1000\,\mathrm{m/s}$ at $20\,\mathrm{m}$ depth. A layer with constant velocity extends down to approximately $65\,\mathrm{m}$. At this depth, a clear interface is found, with a velocity of the lower layer around $1500-1700\,\mathrm{m/s}$. The velocity increases slightly with depth until a velocity contrast at $200\,\mathrm{m}$ depth, which is interpreted as the sediment-bedrock interface. $V_{s,30}$ is equal to $730\,\mathrm{m/s}$, corresponding to ground type B for EC8 and SIA261, i.e. much firmer than expected from the official ground type map (class C). The theoretical SH transfer function and impedance contrast of the quarter-wavelength velocity computed from the inverted profiles show large amplification at high frequencies (above $10\,\mathrm{Hz}$), and moderate amplification at the fundamental resonance frequency ($2.4\,\mathrm{Hz}$). Recordings of the new station will allow to validate these simple models.

Acknowledgements

The authors thank Laura Ermert who helped for the measurements.

References

Sylvette Bonnefoy-Claudet, Fabrice Cotton, and Pierre-Yves Bard. The nature of noise wavefield and its applications for site effects studies. *Earth-Science Reviews*, 79(3-4): 205–227, December 2006. ISSN 00128252. doi: 10.1016/j.earscirev.2006.07.004. URL http://linkinghub.elsevier.com/retrieve/pii/S0012825206001012.

J. Capon. High-Resolution Frequency-Wavenumber Spectrum Analysis. *Proceedings of the IEEE*, 57(8):1408–1418, 1969.

CEN. *Eurocode 8: Design of structures for earthquake resistance - Part 1: General rules, seismic actions and rules for buildings*. European Committee for Standardization, en 1998-1: edition, 2004.

Donat Fäh, Fortunat Kind, and Domenico Giardini. A theoretical investigation of average H / V ratios. *Geophysical Journal International*, 145:535–549, 2001.

Donat Fäh, Gabriela Stamm, and Hans-Balder Havenith. Analysis of three-component ambient vibration array measurements. *Geophysical Journal International*, 172(1):199–213, January 2008. ISSN 0956540X. doi: 10.1111/j.1365-246X.2007.03625.x. URL http://doi.wiley.com/10.1111/j.1365-246X.2007.03625.x.

Donat Fäh, Marc Wathelet, Miriam Kristekova, Hans-Balder Havenith, Brigitte Endrun, Gabriela Stamm, Valerio Poggi, Jan Burjanek, and Cécile Cornou. Using Ellipticity Information for Site Characterisation Using Ellipticity Information for Site Characterisation. Technical report, NERIES JRA4 Task B2, 2009.

Stefan Fritsche and Donat Fäh. The 1946 magnitude 6.1 earthquake in the Valais: site-effects as contributor to the damage. *Swiss Journal of Geosciences*, 102(3):423–439, December 2009. ISSN 1661-8726. doi: 10.1007/s00015-009-1340-2. URL http://www.springerlink.com/index/10.1007/s00015-009-1340-2.

William B. Joyner, Richard E. Warrick, and Thomas E. Fumal. The effect of Quaternary alluvium on strong ground motion in the Coyote Lake, California, earthquake of 1979. *Bulletin of the Seismological Society of America*, 71(4):1333–1349, 1981.

Katsuaki Konno and Tatsuo Ohmachi. Ground-Motion Characteristics Estimated from Spectral Ratio between Horizontal and Vertical Components of Microtremor. *Bulletin of the Seismological Society of America*, 88(1):228–241, 1998.

Valerio Poggi and Donat Fäh. Estimating Rayleigh wave particle motion from three-component array analysis of ambient vibrations. *Geophysical Journal International*, 180(1):251–267, January 2010. ISSN 0956540X. doi: 10.1111/j.1365-246X.2009.04402.x. URL http://doi.wiley.com/10.1111/j.1365-246X.2009.04402.x.

Valerio Poggi, Benjamin Edwards, and Donat Fäh. Characterizing the Vertical-to-Horizontal Ratio of Ground Motion at Soft Sediment-Sites. *Bulletin of the Seismological Society of America*, 102(6), 2012a. doi: 10.1785/0120120039.

Valerio Poggi, Donat Fäh, Jan Burjanek, and Domenico Giardini. The use of Rayleigh-wave ellipticity for site-specific hazard assessment and microzonation: application to the city of Lucerne, Switzerland. *Geophysical Journal International*, 188(3):1154–1172, March 2012b. ISSN 0956540X. doi: 10.1111/j.1365-246X.2011.05305.x. URL `http://doi.wiley.com/10.1111/j.1365-246X.2011.05305.x`.

J.M. Roesset. Fundamentals of soil amplification. In R. J. Hansen, editor, *Seismic Design for Nuclear Power Plants*, pages 183–244. M.I.T. Press, Cambridge, Mass., 1970. ISBN 978-0-262-08041-5. URL `http://mitpress.mit.edu/catalog/item/default.asp?ttype=2\&tid=5998`.

SIA. *SIA 261 Actions sur les structures porteuses*. Société suisse des ingénieurs et des architectes, Zürich, sia 261:20 edition, 2003.

Marc Wathelet. An improved neighborhood algorithm: Parameter conditions and dynamic scaling. *Geophysical Research Letters*, 35(9):1–5, May 2008. ISSN 0094-8276. doi: 10.1029/2008GL033256. URL `http://www.agu.org/pubs/crossref/2008/2008GL033256.shtml`.